

Article

Effects of the PMMA Molecular Weight on the Thermal and Thermo-Oxidative Decomposition as the First Chemical Stage of Flaming Ignition

Antonio Galgano * and Colomba Di Blasi

Dipartimento di Ingegneria Chimica, dei Materiali e della Produzione Industriale, Università degli Studi di Napoli "Federico II", P.le V. Tecchio, 80125 Napoli, Italy; diblasi@unina.it

* Correspondence: agalgano@unina.it; Tel.: +39-081-7682232

Abstract: The piloted and the spontaneous ignition of low and high molecular weight (LMW and HMW) polymethyl methacrylate are simulated using a one-dimensional condensed-gas phase model for constant heat fluxes in the range of 25–150 kW/m². Purely thermal (nitrogen) and thermo-oxidative (air) decomposition is considered, described by a single and four-step kinetics for the low and high molecular weight polymer, respectively. Different optical properties are also examined. The same trends of the ignition time and other ignition parameters are always observed. Due to a more significant role of the chemical kinetics, the effects of the sample molecular weight and reaction atmosphere are higher at low heat fluxes. Times are shorter for the black HMW samples and thermo-oxidative kinetics. For piloted ignition, factors are around 2.8–1.6, whereas for thermal decomposition, they are 1.3–1.2. The corresponding figures are 1.8–1.3 and 1.3–1.1, in the same order, for the spontaneous ignition. Overall, the effects of the molecular weight are more important than those related to the reaction kinetics environment. These differences are confirmed by the comparison between predictions and measurements.

Keywords: PMMA; spontaneous ignition; piloted ignition; modeling; decomposition kinetics; molecular weight



Citation: Galgano, A.; Di Blasi, C. Effects of the PMMA Molecular Weight on the Thermal and Thermo-Oxidative Decomposition as the First Chemical Stage of Flaming Ignition. *Processes* **2024**, *12*, 219. <https://doi.org/10.3390/pr12010219>

Academic Editor: Iztok Golobič

Received: 2 January 2024

Revised: 16 January 2024

Accepted: 17 January 2024

Published: 19 January 2024



Copyright: © 2024 by the authors. Licensee MDPI, Basel, Switzerland. This article is an open access article distributed under the terms and conditions of the Creative Commons Attribution (CC BY) license (<https://creativecommons.org/licenses/by/4.0/>).

1. Introduction

The increasing applications of polymethyl methacrylate (PMMA) in the fields of science and technology, ranging from plastics to electronics [1], are testified by an estimated increase in the global market demand of 7.4% from 2015 to 2025 [2]. An increase in the waste associated with the product's end of life is also expected, which can be exploited by means of thermochemical conversion for energy or other high-value-added products [3–5]. Hence, improvements are required for the understanding of the high-temperature behavior of PMMA, specifically ignition, which is the first important phenomenon of fire spread or air gasification and incineration.

The formulation and experimental validation of mathematical models for simulating the high-temperature behavior of materials represent important steps for the construction of predictive tools to support and integrate costly experimental campaigns [6]. For the development of predictive models, chemical and physical processes should be described with accuracy levels depending on specific requirements for the predictions. In accordance with the literature review reported in [7,8], the first class of PMMA ignition models consists of condensed-phase descriptions coupled with empirical ignition criteria [9–19]. Another model class is based on descriptions of both the condensed and gas phases [7,8,20–29], which do not require the use of empirical criteria. These include both simple unsteady one-dimensional models, which give quantitative information on the main global parameters (e.g., ignition delay time, surface temperature, and volatile mass flux at ignition), and more advanced CFD formulations. In all cases, a critical issue is the need to provide reliable

input data concerning the material properties and the chemical kinetics. In fact, significant variations are observed among the literature values. To quantify the influences of such variability on ignition predictions, an extensive sensitivity analysis has been recently carried out for a one-dimensional solid-gas phase model [7]. For both the spontaneous and the piloted cases, the highest sensitivity concerns the kinetics of polymer decomposition [8]. It is interesting to observe that despite the improvements in the mathematical description of the flaming ignition of PMMA when the empirical criteria of the models [9–19] are substituted by rigorous formulations of conservation equations for mass and energy coupled with combustion kinetics by models [7,8,20–29], a global single-step mechanism is always used for the polymer decomposition into monomers. This kinetics is applicable only to low molecular weight samples.

It has been clearly pointed out [30] that the PMMA decomposition kinetics is influenced by its chemical properties, such as molecular weight, tacticity, branching degrees, and polymerization conditions (for instance, anionic or free radical method). In particular, the PMMA molecular weight determines important features of the decomposition mechanism that turns from a one-stage global reaction (low molecular weight) [7,31–33] into a multistep process (high molecular weight) [17,34]. However, none of the literature models combine multistep decomposition kinetics with the description of either solid phase physical processes only [9–19] or both solid and gas processes [7,8,20–29]. Hence, the subsequent impact of the polymer molecular weight on the ignition behavior has never been investigated.

Another important issue for the PMMA decomposition mechanism, which is not clearly addressed by previous transport models, is the occurrence of the process under inert (thermal decomposition) or oxidative (thermo-oxidative decomposition) ambient [35,36]. The decomposition is accelerated by “the oxygen initiation of the radical degradation chain reaction, taking place at a lower temperature than thermal initiation by C–C bond scission” [36]. On the other hand, the experimental observation during the thermoplastic material combustion in a cone calorimeter reveals [36] that, prior to ignition, the decomposition of the polymer top layer is controlled by oxygen while purely thermal decomposition is taking place in the in-depth molten phase. Finally, once ignition occurs, the flame hinders oxygen diffusion to the surface so that thermal decomposition becomes controlling and higher temperatures are required to produce the same volatile mass flux. It is thus understandable that the role of oxygen requires careful consideration. Again, as anticipated, none of the transport models for PMMA ignition discuss this aspect, except for the model [17], which is focused on the influences of carbon nanotube addition, and model [7], where a comparison is presented between the two kinetics for low molecular weight PMMA only at the moderate heat flux of 50 kW/m².

In summary, the aspects that concern the roles of the molecular weight and the decomposition atmosphere on the polymer decomposition kinetics should be further considered in the formulation of transport models for PMMA flaming ignition to make new advancements with respect to the current state of the art. These are the central topics of this study. In fact, a comprehensive condensed-gas phase model, previously developed by [7,8], is used to investigate the effects of the PMMA molecular weight and thermal or thermo-oxidative decomposition on spontaneous and piloted ignition. More precisely, a single-step or a multistep decomposition mechanism for low and high molecular weight PMMA, respectively, is combined with the description of the main physical processes and the gas-phase combustion of methyl methacrylate (MMA) for conditions that reproduce those of the cone calorimeter and heat fluxes intensities in the range of 25–150 kW/m². The flame structure and the main ignition parameters are predicted. Also, a comparison is provided with the measurements of the ignition delay times and other relevant variables.

2. Decomposition Kinetics of the Selected Materials

This section describes the chief chemical properties of the two PMMA samples whose ignition characteristics are then analyzed. The first sample [17] has a molecular weight of

10^6 g/mol and, in the following, is indicated as HMW PMMA. The second one [31] has a lower molecular weight of 10^5 g/mol and, in the following, is indicated as LMW PMMA. Given the similarity of the mass loss curves of the HMW sample in the nitrogen with those by Ferriol et al. [34], shown by Galgano et al. [17], and the close similarity of the mass loss curves for the LMW sample with those by Kang et al. [33], reported by Galgano and Di Blasi [7], it can be inferred that both samples are produced by free radical polymerization. The kinetic model can be described by a four-step mechanism for the HMW PMMA [17] and by a single-step mechanism for the LMW PMMA [7]. The kinetic parameters, affected by the decomposition environment, are listed in Table 1 for the air (thermo-oxidative kinetics) and nitrogen (purely thermal decomposition). Furthermore, Figure 1 permits a comparison of the predicted mass fractions, Y , and mass loss rates, $-dY/dt$, for the two materials under kinetic control (heating rate of 10 K/min).

Table 1. Kinetic parameters for the LMW and the HMW PMMA samples for decomposition in the air and nitrogen [7,17].

		LMW Air	LMW N ₂	HMW Air	HMW N ₂
1st step	A_{d1} [s ⁻¹]	3.3×10^{20}	6.02×10^{12}	1.3×10^{12}	1.3×10^{12}
	E_{d1} [kJ/mol]	260.6	188	118.0	118.0
	n_{d1}	1.0	1.0	1.4	1.4
	ν_{d1}	1.0	1.0	0.02	0.07
2nd step	A_{d2} [s ⁻¹]			6.0×10^{27}	8.2×10^8
	E_{d2} [kJ/mol]			290.0	112.2
	n_{d2}			2.65	0.97
	ν_{d2}			0.32	0.14
3rd step	A_{d3} [s ⁻¹]			1.3×10^{12}	1.0×10^{13}
	E_{d3} [kJ/mol]			149.4	149.4
	n_{d3}			1.2	1.12
	ν_{d3}			0.23	0.13
4th step	A_{d4} [s ⁻¹]			6.0×10^{13}	2.2×10^{12}
	E_{d4} [kJ/mol]			175.4	175.4
	n_{d4}			2.1	1.25
	ν_{d4}			0.43	0.66

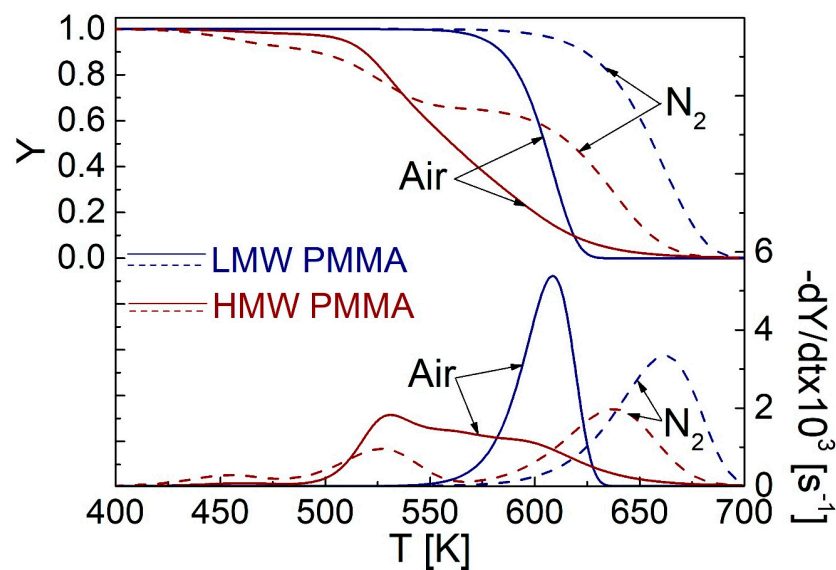


Figure 1. TG and DTG curves for PMMA with low and high molecular weight as predicted by the kinetic models in the air and nitrogen [7,17] for a heating rate of 10 K/min.

As already reported [7,17,36], the reaction environment highly affects the polymer stability. In fact, the peaks of the mass loss rates in the nitrogen are reached at higher temperatures than in the air. More specifically, for the LMW PMMA, the peak in the mass loss rate is reached at about 600 K in the air and 660 K in the nitrogen. For the HMW PMMA, the peak is reached at 530 K in the air and 640 K in the nitrogen.

Furthermore, in agreement with previous studies [34,37], the decomposition reactivity increases with the molecular weight. In fact, not only the peaks of the mass loss rate for the HMW sample are reached at lower temperatures, but the beginning of the mass loss is also anticipated at lower temperatures. The temperature where the residual mass fraction Y is equal to 0.98 is lower by about 160 K in the nitrogen and by 80 K in the air. It is likely that the stabilizing effect with the increase in the molecular weight, noticed by Galgano and Di Blasi [8], is instead attributable to differences in the polymerization process (anionic or thermal polymerization). It is also interesting to observe that for the HMW sample, the amount of monomer released at low temperatures is higher in the nitrogen than in the air (according to the first reaction step, the volatile mass fraction is 0.07 in the nitrogen and 0.02 in the air). Instead, for the LMW PMMA, whose decomposition is described by single-step kinetics, no mass loss is observed at low temperatures. That is, not only the peak rate is attained at higher temperatures but the release of volatiles at low temperatures is also negligible.

3. Mathematical Model of Piloted and Spontaneous Ignition

Details of the unsteady one-dimensional solid-gas mathematical model describing the piloted and spontaneous ignition of PMMA in a cone calorimeter have already been provided elsewhere [7,8] for a one-step decomposition mechanism. In the case of a four-step decomposition mechanism, only a few modifications are required. The complete mathematical model, including the conservation equations, the boundary conditions, and the physicochemical properties, is included in Tables S1–S3 of the Supplementary Materials where the complete nomenclature is also reported. The transport equations for heat and mass transfer for the condensed and the gas phase are based on several assumptions. As for the polymer, it is assumed that the phase change (solid to molten) occurs at an assigned temperature with negligible enthalpy variations. In addition, the condensed phase owns a constant density, while the volume decreases proportionally to the MMA amount generated by the polymer decomposition. However, the interface between the polymer and the gas phase is assumed to be always located at the same place (the sample is moved upward according to the regression rate). Heat transfer by conduction, convection, and radiation is considered. The Beer law is used for the radiation absorption inside the sample, while the two-flux radiation model is used for the heat transfer by radiation in the gas phase, assuming that only MMA absorbs. Radiative absorption by CO_2 and H_2O is neglected following the low concentrations reached in the preignition stage. A single-step second-order kinetic law is assumed for MMA combustion. Only one lumped product is considered with average properties between CO_2 and H_2O , based on the combustion stoichiometry. Mass transfer by convective and diffusive mechanisms is considered, with diffusion coefficients referred to as binary mixtures with air as the second component. Finally, properties depend upon temperature and composition. Finite difference approximations are used to carry out the numerical solution of the equations. The spark is described as a finite-difference cell at the position x_i , which, over an assigned period f , is instantaneously brought at the temperature T_{spark} for a time duration d . The temperature variation related to the spark activity is considered only in the kinetics of the MMA combustion process (chemical spark approximation). The ignition time, t_{ig} , is evaluated as the time when the second derivative of the maximum gas-phase temperature, T_{gmax} , is zero and its values continue to increase. Instead, for spontaneous ignition, the condition of the second derivative of T_{gmax} equal to zero is sufficient to identify the ignition time. Input data are the same used by Galgano and Di Blasi [7,8] and are listed in Table 2 [10,11,21,23,29,32,38–42], except for the kinetic data (listed in Table 1). Different optical properties are also considered, corresponding to clear

and black PMMA, with differences in the absorption coefficient, β_s , and emissivity, e_s , as reported in Table 2.

Table 2. Values of the input data for the numerical simulations [7,8].

Parameters	Values	References
A_c	1.6×10^{15}	[38]
D_{MMA0}	8.83×10^{-6}	[39]
D_{O20}	2.075×10^{-5}	[40]
D_{P0}	1.85×10^{-5}	[40]
d	0.005	[23]
E_c	180	[38]
f	0.1	[23]
M_{MMA}	100.1	[40]
T_{spark}	1623	[29]
T_{trans}	403	[10]
x_i	0.013	[23]
β_g	4.0	[21]
Δh_c	2.592×10^7	[21]
Δh_d	8.7×10^5	[41]
ρ_p	1200	[10]
ν_c	1.92	[40]
	Clear PMMA	
e_s	0.86	[32]
β_s	1870	[42]
	Black PMMA	
e_s	0.945	[11]
β_s	2620	[42]

4. Results and Discussion

The main output variables of the piloted ignition are first compared for the cases of black LMW and HMW PMMA with thermo-oxidative and purely thermal decomposition kinetics for heat flux, Q , of 50 kW/m^2 . Then, the analysis is extended to the range of heat fluxes $25\text{--}150 \text{ kW/m}^2$ for both piloted and spontaneous ignition. The effects of the optical properties are also evaluated. Finally, the model predictions are compared with measured ignition times and corresponding surface temperatures and mass fluxes.

4.1. Piloted Ignition Characteristics for $Q = 50 \text{ kW/m}^2$

The ignition characteristics for black LMW and HMW PMMA predicted using the purely thermal (in the nitrogen) and thermo-oxidative (in the air) decomposition kinetics of Table 1 and an incident heat flux of 50 kW/m^2 are summarized in Figures 2 and 3 and Table 3. More specifically, Figure 2 shows the temperature profiles at ignition for the four cases while Figure 3 shows the profiles of monomer and oxygen mass fraction, Y_{MMA} and Y_{O_2} , and the combustion rate, ω_c , at the ignition time. Table 3 lists the main output variables at ignition, such as ignition time, t_{ig} , and the corresponding surface temperature, T_{sig} , monomer mass flux, m_{sig} , polymer thermal penetration depth, δ_{ig} , maximum gas-phase temperature, T_{gmaxig} , and the corresponding position, x_{ig} , monomer to oxygen mass fraction ratio at the ignition position, r_{ig} , and the width of the combustion zone, w_{ig} , defined as the gas-phase region where the combustion rate is higher than a threshold value of $0.5 \text{ kg/m}^3\text{s}$ [8].

At first glance, it is evident that, in all cases, the ignition position is almost coincident with that of the spark. In addition, the ignition time, t_{ig} , is shorter for the HMW PMMA for both thermal and thermo-oxidative decomposition kinetics, showing that ignition is not related to the peak of the mass loss rate, reported in Figure 1, but is related to the release of MMA at low temperatures. Furthermore, longer ignition times cause a widening of the

gas-phase temperature profile and a lower peak, most likely due to a larger consumption of the MMA concentration by the spark activity during the preignition stage.

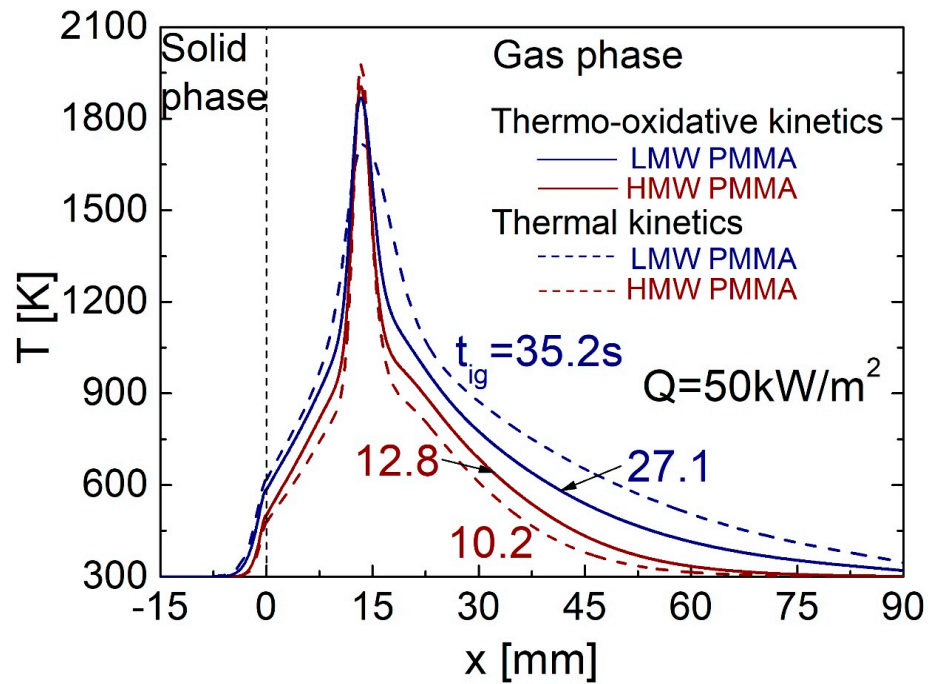


Figure 2. Spatial profiles of the solid- and gas-phase temperature at the ignition time as predicted for piloted ignition of black LMW and HMW PMMA with thermo-oxidative decomposition kinetics (solid lines) and purely thermal decomposition kinetics (dashed lines) ($Q = 50 \text{ kW/m}^2$).

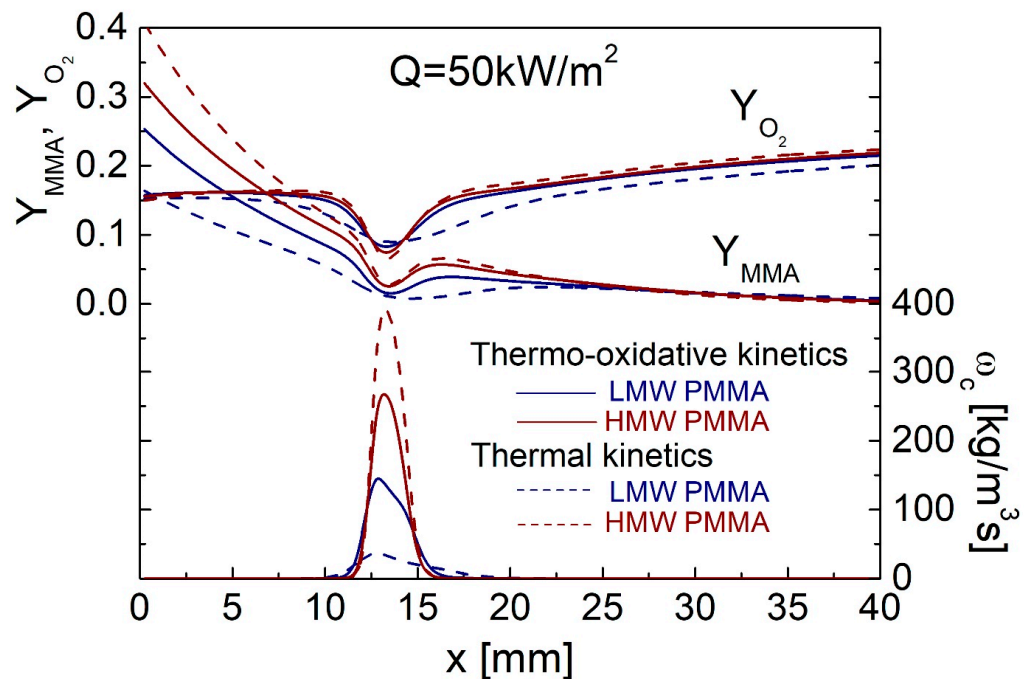


Figure 3. Spatial profiles of the monomer, Y_{MMA} , and oxygen, Y_{O_2} , mass fractions and the combustion reaction rate, ω_c , at the ignition time as predicted for piloted ignition of black LMW and HMW PMMA with thermo-oxidative decomposition kinetics (solid lines) and purely thermal decomposition kinetics (dashed lines) ($Q = 50 \text{ kW/m}^2$).

Table 3. Ignition time, t_{ig} , and the corresponding surface temperature, T_{sig} , mass flux, m_{sig} , thermal depth, δ_{ig} , maximum gas-phase temperature, T_{gmaxig} , the position of the flaming ignition point, x_{ig} , monomer to oxygen mass fraction ratio at the ignition position, r_{ig} , and the width of the gas-phase reaction zone, w_{ig} , as predicted for the piloted ignition of black LMW and HMW PMMA with purely thermal and thermo-oxidative decomposition kinetics ($Q = 50 \text{ kW/m}^2$).

Material	Decomposition Kinetics	t_{ig} [s]	T_{sig} [K]	m_{sig} [$\text{g/m}^2 \text{ s}$]	δ_{ig} [mm]	x_{max} [mm]	T_{gmaxig} [K]	r_{ig}	w_{ig} [mm]
Black LMW PMMA	Thermal	35.2475	616	0.35	4.04	13.8	1719	0.12	10.9
	Thermo-oxidative	27.1059	584	0.73	3.47	13.2	1878	0.16	8.1
Black HMW PMMA	Thermal	10.2063	478	1.56	2.0	13.2	2003	0.47	5.1
	Thermo-oxidative	12.8059	501	0.97	2.27	13.2	1927	0.34	6.2

A quantitative analysis of the results shows that an ignition time t_{ig} of 12.8 s is predicted for the HMW PMMA with thermo-oxidative kinetics, corresponding to a surface temperature T_{sig} of 501 K. The ignition time predicted for the LMW PMMA is longer by a factor of 2.1 and T_{sig} is higher by 83 K. Using purely thermal kinetics, t_{ig} is reduced by a factor of about 1.25 for the HMW PMMA with T_{sig} decreased by 23 K. Instead, a longer ignition time is predicted for the LMW PMMA by a factor of 1.3 with T_{sig} increased by 32 K.

Despite the significant differences in the kinetic models, it is interesting to observe that the qualitative trends of the main output variables on the dependence of the ignition time are the same as observed by Galgano and Di Blasi [8] with the one-step kinetic model. In fact, following the increase in the exposure time to the heat flux, the thermal penetration depth, δ_{ig} , increases from 2.0 mm to 4.0 mm; instead, the monomer mass flux, m_{sig} , decreases by a factor of about 4.4 (from 1.56 $\text{g/m}^2 \text{ s}$ to 0.35 $\text{g/m}^2 \text{ s}$), probably because the temperatures of the solid surface and the gas phase increase, as shown in Figure 2, requiring a lower amount of MMA to establish ignition conditions. This is also shown by the profiles of MMA mass fraction, Y_{MMA} , in Figure 3. Following the trend of the mass flux, the monomer to oxygen mass fraction ratio, r_{ig} , also decreases by a factor of 3.6 (from 0.43 to 0.12). Longer ignition times are also characterized by a decrease in the maximum gas-phase temperature, T_{gmaxig} , up to about 300 K, following the same trend already observed by Galgano and Di Blasi [8], due to the longer spark activity causing higher monomer consumption. Due to the shape of the temperature profiles, almost coincident values are reached for the four cases at about 12.5 mm and 14.5 mm, while maximum deviations up to 400 K and 500 K are evaluated around 11 mm and 17 mm, respectively. Furthermore, the width of the temperature peak enlarges, and consequently, the width of the gas-phase combustion zone, w_{ig} , also becomes wider, increasing by a factor of about 2.1. The maximum of the combustion reaction rate, ω_c , decreases by about one order of magnitude.

To also evaluate the effects of the optical properties, simulations have been carried out with clear LMW and HMW PMMA, and the results are summarized in Table 4. As expected, due to the lower absorption coefficient (1870 m^{-1} vs. 2620 m^{-1}) and surface emissivity (0.86 vs. 0.945), longer ignition times are predicted. However, the factor of increase is quite small, with a value of around 1.2 for all cases with a roughly constant factor of decrease of 1.2–1.3 for the mass flux, m_{sig} , and 1.2–1.5 for the monomer to oxygen mass fraction ratio at the ignition position, r_{ig} . The surface temperatures, T_{sig} , are almost the same (lower by about 5–9 K) due to compensation between longer exposure times to the external heat flux and reduced values of the absorbance and surface emissivity. The position of the maximum temperature in the gas phase, x_{ig} , is again the same as predicted for black PMMA (nearly coincident with the position of the spark), but maximum temperatures, T_{gmaxig} , are slightly lower (about 20–70 K) owing to the enhanced activity of the spark, which enlarges the reaction zone, with higher w_{ig} by 5–10%.

Table 4. Ignition time, t_{ig} , and the corresponding surface temperature, T_{sig} , mass flux, m_{sig} , thermal depth, δ_{ig} , maximum gas-phase temperature, T_{gmaxig} , the position of the flaming ignition point, x_{ig} , monomer to oxygen mass fraction ratio at the ignition position, r_{ig} , and the width of the gas-phase reaction zone, w_{ig} , as predicted for the piloted ignition of clear LMW and HMW PMMA with purely thermal and thermo-oxidative decomposition kinetics ($Q = 50 \text{ kW/m}^2$).

Material	Decomposition Kinetics	t_{ig} [s]	T_{sig} [K]	m_{sig} [$\text{g/m}^2 \text{ s}$]	δ_{ig} [mm]	x_{max} [mm]	T_{gmaxig} [K]	r_{ig}	w_{ig} [mm]
Clear LMW PMMA	Thermal	44.2545	610	0.30	4.64	13.8	1689	0.098	11.4
	Thermo-oxidative	34.5168	579	0.58	4.04	13.8	1810	0.13	8.8
Clear HMW PMMA	Thermal	12.8053	470	1.18	2.37	13.2	1957	0.32	5.6
	Thermo-oxidative	16.0071	492	0.75	2.67	13.2	1904	0.26	6.8

To summarize, given that the ignition process is controlled by the release of MMA at low temperatures, as shown by the low surface temperatures, shorter ignition times are predicted using thermo-oxidative decomposition kinetics only for the LMW PMMA. In fact, only in this case, decomposition is shifted at lower temperatures. Furthermore, the ignition times are longer for clear PMMA by factors that are independent of decomposition kinetics.

4.2. Piloted Ignition Characteristics for Q Values in the Range of 25–150 kW/m^2

In this section, the effects of the heat flux intensity in the range of 25–150 kW/m^2 on the piloted ignition characteristics of black LMW and HMW PMMA are studied. For both samples, purely thermal and thermo-oxidative kinetics are considered. The values of the main output variables (t_{ig} , T_{sig} , m_{sig} , δ_{ig} , x_{ig} , T_{gmaxig} , r_{ig} , and w_{ig}) are shown in Figure 4. In all cases, the predicted values of each output variable are in the same order predicted at the reference heat flux of 50 kW/m^2 , except for m_{sig} and r_{ig} at heat fluxes higher than 120 kW/m^2 and T_{gmaxig} , as specified below. A qualitative description of the results is first provided. Then, quantitative comparisons between predictions are carried out for the LMW and HMW PMMA with thermo-oxidative kinetics. Finally, for each PMMA sample, the effects of the environment on the decomposition kinetics are assessed.

As already shown for the LMW PMMA with thermo-oxidative kinetics [7], t_{ig} continuously decreases while T_{sig} and m_{sig} increase. Shorter ignition times are also associated with shorter δ_{ig} , while higher mass fluxes are associated with higher r_{ig} . The ignition position, x_{ig} , moves closer to the spark position, and the width of the combustion reaction zone, w_{ig} , becomes smaller due to reduced fuel consumption in the preignition stage and faster combustion rates. The T_{gmaxig} parameter is the only one not showing a monotone trend. In fact, it initially increases, again due to a reduced activity of the combustion reaction in the preignition stage, and then decreases showing that the MMA combustion rate is sufficiently high to also activate ignition at lower temperatures.

The quantitative comparison between the piloted ignition characteristics for the LMW and HMW PMMA with thermo-oxidative kinetics shows that the differences between the predicted ignition times decrease as the heat flux increases, due to a reduced role of kinetic control compared with transport phenomena. In fact, the ignition time, t_{ig} , predicted for the HMW PMMA is shorter by factors of 2.8–1.6 with respect to that predicted for the LMW PMMA, while the corresponding δ_{ig} is shorter by factors of 1.9–1.2. Because of the higher reactivity of the HMW PMMA, the predicted surface temperatures, T_{sig} , are lower by about 90–70 K. However, the mass flux, m_{sig} , and r_{ig} are higher by a nearly constant factor of about 1.3 (lower decomposition temperatures require higher amounts of MMA released to reach the ignition conditions). Longer ignition times cause a longer distance of the ignition position, x_{ig} , due to oxygen consumption during the preignition period. Anyway, maximum distances for the LMW and HMW PMMA at 25 kW/m^2 are 15.2 mm and 14 mm, respectively. The smallest value of about 13 mm is reached at 75 kW/m^2 and 40 kW/m^2 , respectively, and then it is constant for higher heat fluxes. The shorter

ignition times predicted for the HMW PMMA also cause a lower consumption of MMA concentration in the gas phase during the preignition period. Thus, the temperatures in the gas phase are lower and the thickness of the combustion zone, w_{ig} , is smaller (by a factor of about 1.2–1.3). As observed, T_{gmaxig} initially increases, reaches a maximum of about 2000 K, and then decreases. Up to applications of heat fluxes of 85 kW/m^2 , higher values are obtained for the HMW PMMA, again due to lower ignition times and, consequently, reduced combustion activity during the preignition period. Instead, for higher heat fluxes, T_{gmaxig} is lower for the HMW PMMA, as the flame becomes very thin. It can be observed that the maximum of T_{gmaxig} is reached for a threshold value of about 5 mm for w_{ig} .

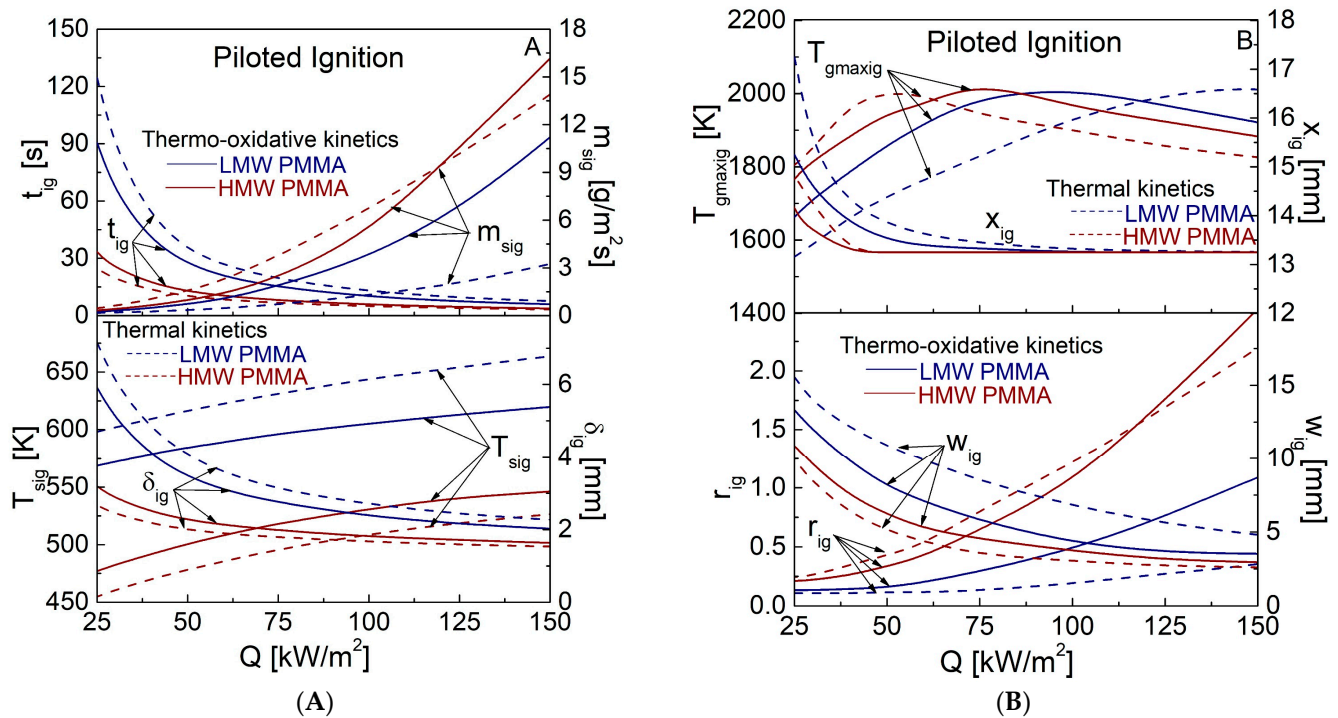


Figure 4. Ignition time, t_{ig} , and the corresponding surface temperature, T_{sig} , mass flux, m_{sig} , thermal depth, δ_{ig} , (A) maximum gas-phase temperature, T_{gmaxig} , the position of the flaming ignition point, x_{ig} , monomer to oxygen mass fraction ratio at the ignition position, r_{ig} , and the width of the gas-phase reaction zone, w_{ig} , (B) as predicted for the piloted ignition of black LMW and HMW PMMA with thermo-oxidative decomposition kinetics (solid lines) and purely thermal decomposition kinetics (dashed lines) vs. the thermal irradiance, Q .

The following examines the effects of purely thermal decomposition kinetics on the predicted piloted ignition variables for both the LMW and HMW PMMA with respect to the case of thermo-oxidative decomposition kinetics. In the range of heat fluxes $25\text{--}150 \text{ kW/m}^2$, t_{ig} is longer by factors of about 1.4–1.3 for the LMW PMMA and lower by factors of about 1.3–1.2 for the HMW PMMA. The parameter δ_{ig} follows the same trend as t_{ig} ; thus, it is thicker for the LMW PMMA and thinner for the HMW PMMA by factors of about 1.2–1.1. Instead, the predicted surface temperature T_{sig} is higher by about 30–45 K for the LMW PMMA and lower by about 20 K for the HMW PMMA. The predicted mass loss flux, m_{sig} , shows the largest variations with values lower by factors of 1.4–3.4 for the LMW PMMA. For the HMW PMMA, higher values of m_{sig} are predicted for heat fluxes below 120 kW/m^2 up to a factor of 1.6; however, for higher irradiance intensities, lower values are predicted up to a factor of 1.2. Again, the predictions of r_{ig} are qualitatively similar to those of m_{sig} . Lower values by factors of 1.2–3.2 are predicted for the LMW PMMA, while higher values are predicted for the HMW PMMA (factors of 1.3–1.1). The thickness of the combustion zone, w_{ig} , is larger by a factor of 1.2–1.4 for the LMW PMMA and smaller by a factor of 1.1–1.2 for the HMW PMMA. A maximum gas temperature value of

2000 K is also reached using purely thermal kinetics for both the LMW and HMW PMMA. It is anticipated for a heat flux of 40 kW/m² in the first case and delayed in the latter case for a heat flux of 140 kW/m² (vs. 75 kW/m² and 100 kW/m² for thermo-oxidative kinetics, respectively).

It can be observed that while the variations in the predicted ignition times induced by the type of decomposition kinetics decrease with the heat flux intensity, the effects on some variables remain constant or increase. It is likely that this result is a consequence of the reduced thickness of the flame. In fact, when the flame thickness is small, the heat released by the combustion process is lower, so a longer time is needed to reach the ignition conditions, and m_{sig} , T_{sig} , and r_{ig} increase more. This effect is more evident for the LMW PMMA as for the HMW PMMA, ignition is extremely fast for both kinetics.

In summary, the differences induced by purely thermal kinetics are globally less strong than those induced by the differences in molecular weight. Furthermore, the effects of the decomposition kinetics are generally more evident on the LMW PMMA than on the HMW PMMA due to reduced ignition times in the latter case and, consequently, to the reduced control of the decomposition kinetics on the ignition process compared with the transport phenomena.

4.3. Spontaneous Ignition Characteristics for Q in the Range of 25–150 kW/m²

This section discusses the effects of the decomposition environment and the polymer molecular weight on the spontaneous ignition characteristics of black PMMA in the range of heat fluxes 25–150 kW/m². The main ignition parameters defined before are reported in Figure 5. It is shown that they follow the same qualitative trend observed for the piloted ignition, except for the maximum gas-phase temperature, T_{gmaxig} , and the ignition position, x_{ig} . In fact, T_{gmaxig} continuously decreases, most likely because of the higher mass fluxes, enabling ignition at lower temperatures. Instead, the ignition position, x_{ig} , continuously decreases in some cases (thermal kinetics), while in other cases, it first decreases and then slightly increases (thermo-oxidative kinetics). Due to the absence of a pilot, ignition occurs where adequate conditions of temperature and species concentration are reached.

In the following, a quantitative comparison is made between the LMW and the HMW PMMA predictions with thermo-oxidative kinetics. Then, the effects of the decomposition kinetics (thermo-oxidative vs. purely thermal kinetics) for both the LMW and the HMW PMMA samples are assessed.

As already observed for the piloted ignition, the differences between the predicted ignition times for the LMW and the HMW PMMA decrease as the heat flux increases. In fact, the ignition times, t_{ig} , predicted for the HMW PMMA are shorter by factors of 1.8–1.3 with respect to those predicted for the LMW PMMA, while the corresponding δ_{ig} is shorter by factors of 1.5–1.2. Owing to the higher reactivity of the HMW PMMA, the predicted surface temperatures, T_{sig} , are lower by about 60 K–70 K. Instead, the mass flux, m_{sig} , and r_{ig} are higher by a factor of 1.9–1.2. In contrast with what was observed for the piloted ignition, the ignition position, x_{ig} , predicted for the spontaneous ignition is larger for the HMW PMMA. The mass release at lower temperatures with the absence of a pilot causes the ideal conditions for ignition to be reached far from the polymer surface. With the increase in the heat flux, the surface temperature increases; thus, x_{ig} decreases from 47 mm to 41 mm in the range of $Q = 25$ –50 kW/m². However, for higher heat fluxes, x_{ig} slightly increases from 41 mm to 44 mm, probably because the effect of a thinner flame outweighs that of a higher surface temperature. Ignition requires a higher amount of MMA in the gas phase. Thus, the mass flux increases, pushing ahead the ignition position. The same qualitative predictions are obtained for the LMW PMMA, with an ignition position that is shorter by 8–14 mm.

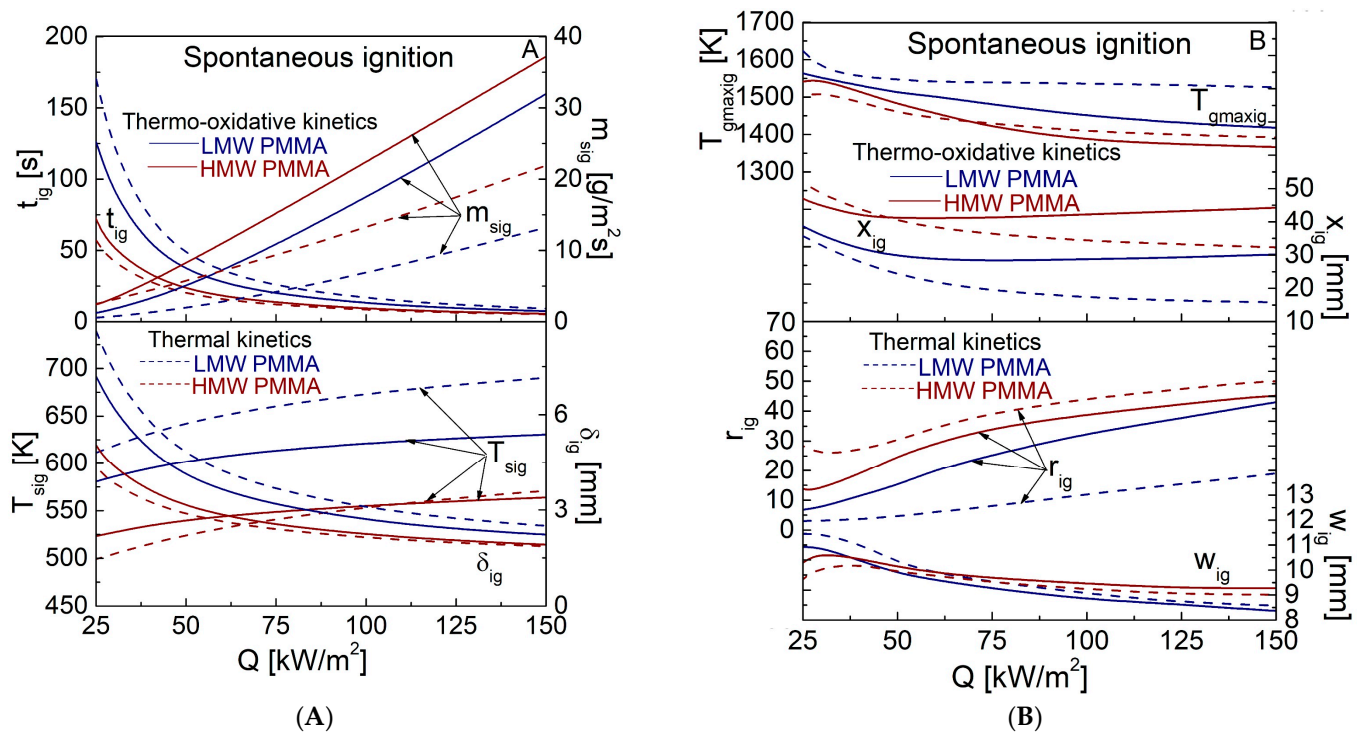


Figure 5. Ignition time, t_{ig} , and the corresponding surface temperature, T_{sig} , mass flux, m_{sig} , thermal depth, δ_{ig} , (A) maximum gas-phase temperature, T_{gmaxig} , the position of the flaming ignition point, x_{ig} , monomer to oxygen mass fraction ratio at the ignition position, r_{ig} , and the width of the gas-phase reaction zone, w_{ig} , (B) as predicted for the spontaneous ignition of black LMW and HMW PMMA with thermo-oxidative decomposition kinetics (solid lines) and purely thermal decomposition kinetics (dashed lines) vs. the heat flux, Q .

The shorter ignition times predicted for the HMW PMMA cause a lower heating of the gas phase. However, the higher mass fluxes, although released at lower surface temperatures, permit the attainment of ignition conditions with slightly lower gas-phase temperatures. Indeed, T_{gmaxig} predicted for the HMW PMMA is lower by 20–50 K with respect to the LMW PMMA. The thickness of the combustion zone, w_{ig} , is quite independent of the molecular weight. In fact, values vary in the range of 8–11 mm and 9–11 mm for the LMW and HMW PMMA, respectively.

The following discusses variations of the ignition parameters predicted with purely thermal kinetics with respect to those predicted with thermo-oxidative kinetics for the LMW and HMW PMMA in the range of heat fluxes 25–150 kW/m^2 . The ignition time, t_{ig} , is longer by factors of about 1.4–1.2 for the LMW PMMA and lower by factors of about 1.3–1.1 in the other case. The penetration depth, δ_{ig} , follows the same trend as t_{ig} ; thus, it is thicker for the LMW PMMA by factors of about 1.2–1.1 and thinner for the HMW PMMA by factors of about 1.2–1.0. The surface temperature T_{sig} is higher by about 30–60 K for the LMW PMMA. For the HMW PMMA, lower values (around 25 K) are predicted for $Q = 25 \text{ kW/m}^2$, but the difference decreases with the heat flux. Slightly higher values are predicted for Q higher than 110 kW/m^2 , up to about 10 K, probably because of the lower distance of the ignition position x_{ig} from the surface (up to about 12 mm for the HMW PMMA and 14 mm for the LMW PMMA).

Similarly, with the trend observed for the piloted ignition, the predicted mass loss flux, m_{sig} , is lower by factors of 2.2–2.4 for the LMW PMMA. Surprisingly, shorter values, by factors of up to 1.7, are also predicted for the HMW PMMA, most likely because the polymer decomposition begins at lower temperatures and the ignition position is closer to the polymer surface. Lower values of r_{ig} are also predicted for the LMW PMMA by a factor of about 2.2, following the same trend of m_{sig} , as observed for piloted ignition. Instead,

higher values by factors of 2.2–1.1 are predicted for the HMW PMMA. In this case, the trend is not the one observed for m_{sig} , again owing to the lower distance of the ignition position from the polymer surface, which causes higher MMA concentrations.

Negligible differences are observed for the thickness of the combustion zone, w_{ig} , in both cases. Limited effects on the maximum gas-phase temperature T_{gmaxig} are also predicted, with maximum variations of about 40 K for the HMW PMMA and 110 K for the LMW PMMA.

In summary, for the spontaneous ignition, the effects of the molecular weight on the predictions of t_{ig} , T_{sig} , and δ_{ig} are higher with respect to those induced by the environment of the decomposition kinetics (similarly to piloted ignition), which instead has a greater influence on m_{sig} , x_{ig} and r_{ig} , mainly for the LMW PMMA.

4.4. Effects of the Optical Properties

The effects of the different optical properties of the LMW and HMW PMMA are studied varying the heating flux intensity in the range of 25–150 kW/m². For simplicity, only the piloted ignition of black and clear PMMA is considered using thermo-oxidative kinetics.

The qualitative trends predicted for clear PMMA, shown in Figure 6, are the same as predicted for black PMMA with only some quantitative differences, almost independent of the molecular weight. The ignition time, t_{ig} , predicted for clear PMMA is longer by a factor of about 1.2–1.3. Despite the longer exposure times, the surface temperature, T_{sig} , for clear PMMA is lower, due to the lower surface emissivity and radiation absorption in the subsurface layers of the polymer. Anyway, the differences do not exceed 10 K for both cases. The penetration depth, δ_{ig} , is higher by factors of 1.1–1.2. Slightly higher variations are predicted for the mass flux, m_{sig} , which is lower by factors of 1.1–1.8. Similar trends are also predicted for r_{ig} , with predicted values lower by factors of 1.0–2.0. The smaller differences observed at longer ignition times (already shown for the LMW PMMA [7]) probably depend on a larger increase in the internal heat dispersion for black PMMA at low heat fluxes. The deviations in the other output variables (x_{ig} , T_{gmaxig} , and w_{ig}) are negligible.

4.5. Comparison between Predictions and Measurements

The piloted ignition time, t_{ig} , and the corresponding surface temperature, T_{sig} , and mass flux, m_{sig} , predicted by the mathematical model for black and clear LMW and HMW PMMA with purely thermal and thermo-oxidative decomposition kinetics are plotted in Figures 7–9, respectively, where they are compared with values measured in cone calorimeters or similar radiant systems with different igniters (spark, heated wire, or pilot flame) for samples with different properties (production process and polymerization degree) [10,17,23,26,43–54].

Almost all the experimental data have already been used to validate the ignition model for the LMW PMMA by Galgano and Di Blasi [7,8]. Despite the wide dispersion of the experimental data, a good agreement between measured and simulated ignition times is found if black PMMA is considered as most of the experimental data refer to a polymer with these optical properties. A better agreement is found with thermo-oxidative decomposition kinetics. Only data by Galgano et al. [17] explicitly refer to clear HMW PMMA. It can be observed that the ignition times measured for HMW PMMA [17] are much shorter, confirming that the other experimental data refer to PMMA samples with lower molecular weight or maybe obtained with different polymerization processes and, thus, characterized by different kinetic parameters and/or decomposition schemes. A good agreement is found between predictions and measurements for clear HMW PMMA. This is an important result showing that although there could be compensation effects among kinetics, absorption properties, and spark temperature [8], the selected input data are reasonably correct.

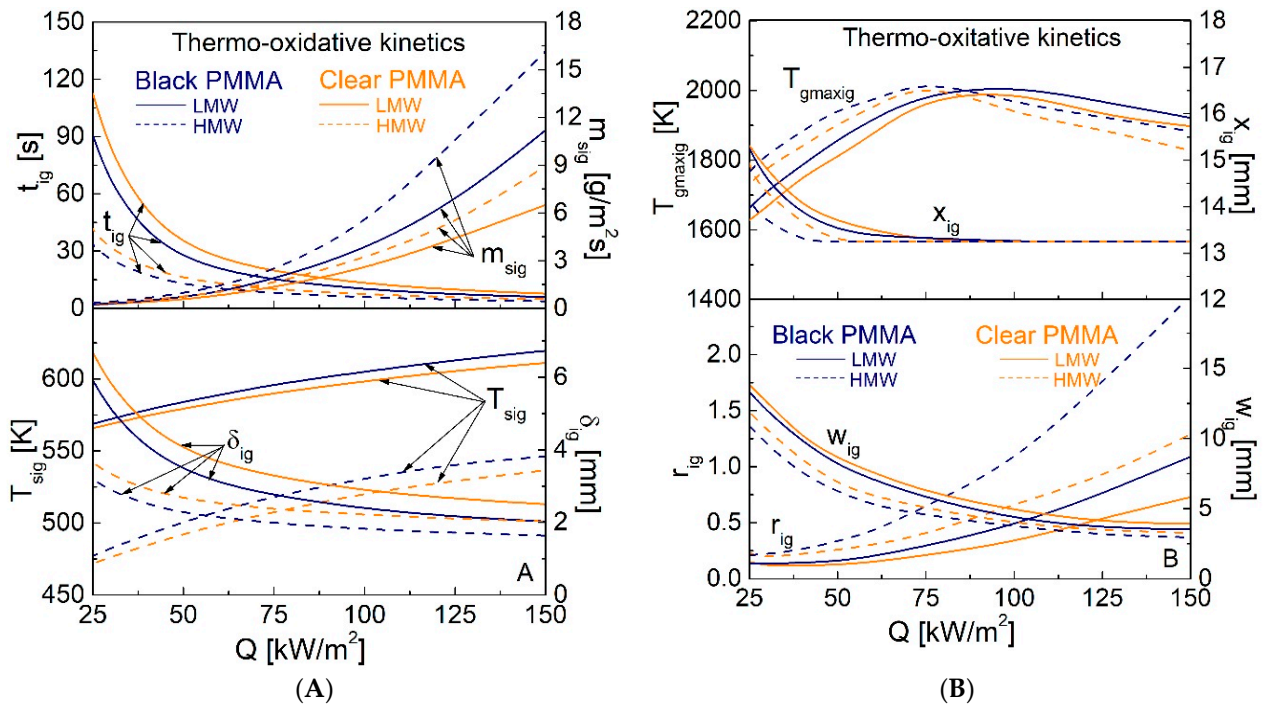


Figure 6. Ignition time, t_{ig} , and the corresponding surface temperature, T_{sig} , mass flux, m_{sig} , thermal depth, δ_{ig} , (A) maximum gas-phase temperature, T_{gmaxig} , the position of the flaming ignition point, x_{ig} , monomer to oxygen mass fraction ratio at the ignition position, r_{ig} , and the width of the gas-phase reaction zone, w_{ig} , (B) as predicted for the piloted ignition of clear and black LMW (solid lines) and HMW PMMA (dashed lines) with thermo-oxidative decomposition kinetics vs. the heat flux, Q .

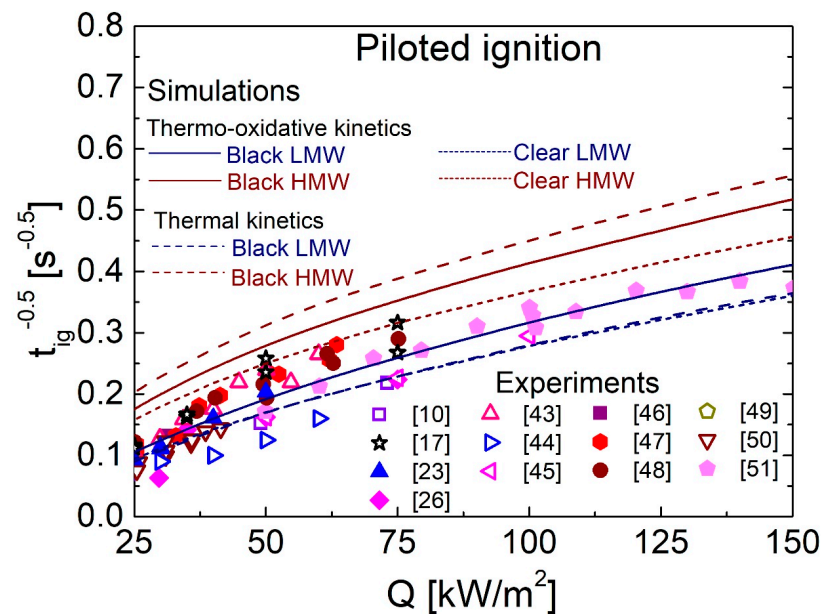


Figure 7. The inverse of the square root of the piloted ignition delay time as a function of the heat flux, Q , as predicted for black and clear LMW (solid and dotted blue lines) and HMW (solid and dotted brown lines) PMMA with thermo-oxidative decomposition kinetics and for black LMW (dashed blue line) and HMW (dashed brown line) PMMA with purely thermal decomposition kinetics. Experimental data (symbols) derived from the literature are also reported. (see Refs. [10,17,23,26,43–51]).

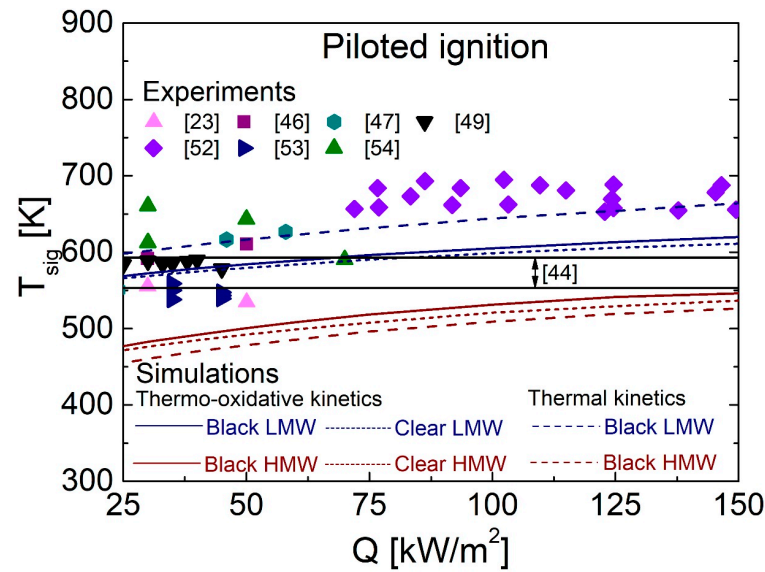


Figure 8. Surface temperature at ignition, T_{sig} , vs. heat flux, Q , as predicted for black and clear LMW (solid and dotted blue lines) and HMW (solid and dotted brown lines) PMMA with thermo-oxidative decomposition kinetics and for black LMW (dashed blue line) and HMW (dashed brown line) PMMA with purely thermal decomposition kinetics. Several experimental data (symbols) derived from the literature are also reported with the range of critical values [44] typically used by empirical criteria. (See Refs. [23,44,46,47,49,52–54]).

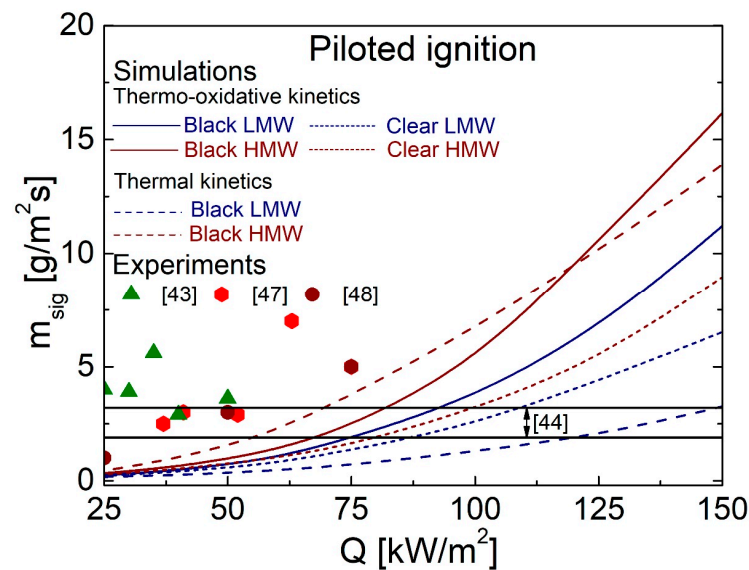


Figure 9. Surface mass flux at ignition, m_{sig} , vs. heat flux, Q , as predicted for black and clear LMW (solid and dotted blue lines) and HMW (solid and dotted brown lines) PMMA with thermo-oxidative decomposition kinetics and for black LMW (dashed blue line) and HMW (dashed brown line) PMMA with purely thermal decomposition kinetics. Several experimental data (symbols) derived from the literature are also reported with the range of critical values [44] typically used by empirical criteria. (See Refs. [43,44,47,48]).

As for T_{sig} (Figure 8), only the values predicted for the LMW PMMA belong to the experimental range of 550–700 K. Instead, much lower values are predicted for the HMW PMMA, in the range of 450–550 K, which is also below the range of critical values applied by empirical criteria for piloted ignition (553–593 K) [44]. Thus, again, it is likely that the experimental data of surface temperatures (and the range of critical values) are not specific

to the HMW PMMA. As already observed before, the effect of the optical properties on the predicted T_{sig} is negligible.

Instead, it is interesting to observe that a better agreement between experimental and predicted surface temperatures is obtained using thermo-oxidative decomposition kinetics for irradiance intensities below 75 kW/m^2 . Instead, for higher heat fluxes, the agreement is more accurate if purely thermal decomposition kinetics is used. It should be observed that though for high irradiance intensities decomposition mostly occurs across the most external layers of the polymer, owing to higher intensities of the efflux flows, the oxygen concentration at the polymer surface at ignition is smaller. Furthermore, the experimental data available for high heat fluxes belong to the same study [52], so it is plausible that further experiments are needed to clarify this aspect.

As for m_{sig} (Figure 9), the predicted values are, for all cases, significantly below the experimental values for heat fluxes in the range of $25\text{--}75 \text{ kW/m}^2$. At higher heat fluxes no measurements are available while predictions rapidly increase. Thus, only in a very narrow range of heat fluxes, does the predicted m_{sig} fall within the range of critical values typically used by empirical criteria [44].

A comparison between measured and predicted t_{ig} , T_{sig} , and m_{sig} in the range of heat fluxes $25\text{--}150 \text{ kW/m}^2$ is also carried out for the spontaneous ignition in Figures 10–12, respectively. As most of the measurements [23,25,28,52,55–58] refer to clear PMMA, simulations have been carried out for clear LMW and HMW PMMA with thermal and thermo-oxidative kinetics, but results for black LMW and HMW PMMA with thermo-oxidative kinetics are also included for comparison. As expected, it can be observed that the best agreement between predicted and measured t_{ig} is obtained with the data of clear LMW PMMA with thermo-oxidative kinetics. As previously shown, the differences introduced by different optical properties or the different decomposition kinetics are quite limited and the results are still in the range of the experimental values. Instead, the predictions of the spontaneous ignition times for the HMW PMMA are always shorter with respect to measurements over the entire range of heat fluxes.

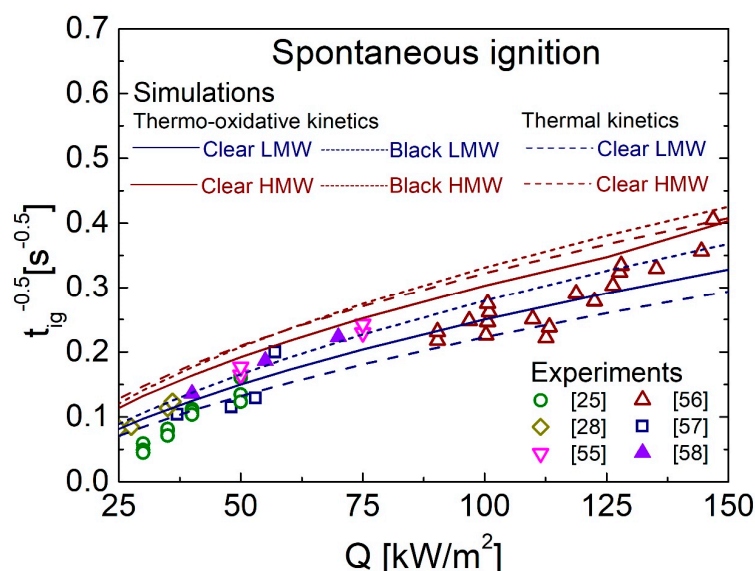


Figure 10. The inverse of the square root of the spontaneous ignition delay time as a function of the heat flux, Q , as predicted for clear and black LMW (solid and dotted blue lines) and HMW (solid and dotted brown lines) PMMA with thermo-oxidative decomposition kinetics and for clear LMW (dashed blue line) and HMW (dashed brown line) PMMA with purely thermal decomposition kinetics. Experimental data (symbols) derived from the literature are also reported. (See Refs. [25,28,55–58]).

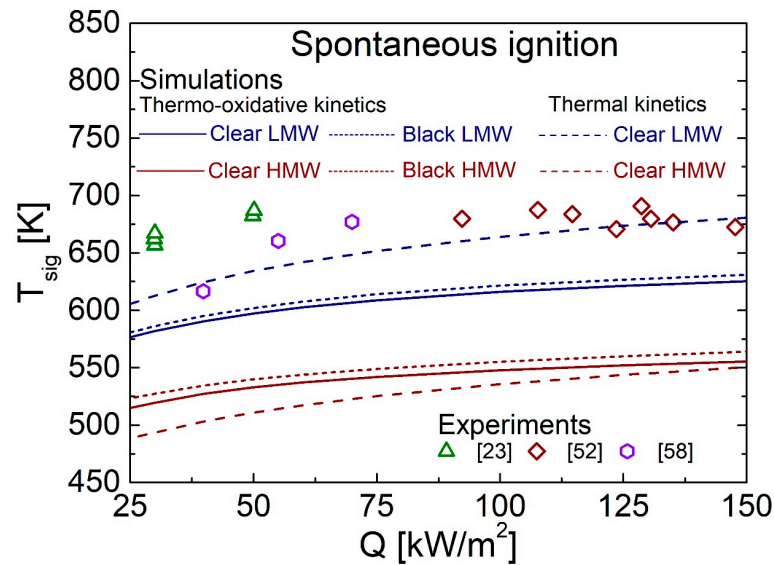


Figure 11. Surface temperature at ignition, T_{sig} , vs. heat flux, Q , as predicted for clear and black LMW (solid and dotted blue lines) and HMW (solid and dotted brown lines) PMMA with thermo-oxidative decomposition kinetics and for clear LMW (dashed blue line) and HMW (dashed brown line) PMMA with purely thermal decomposition kinetics. Experimental data (symbols) derived from the literature are also reported. (See Refs. [23,52,58]).

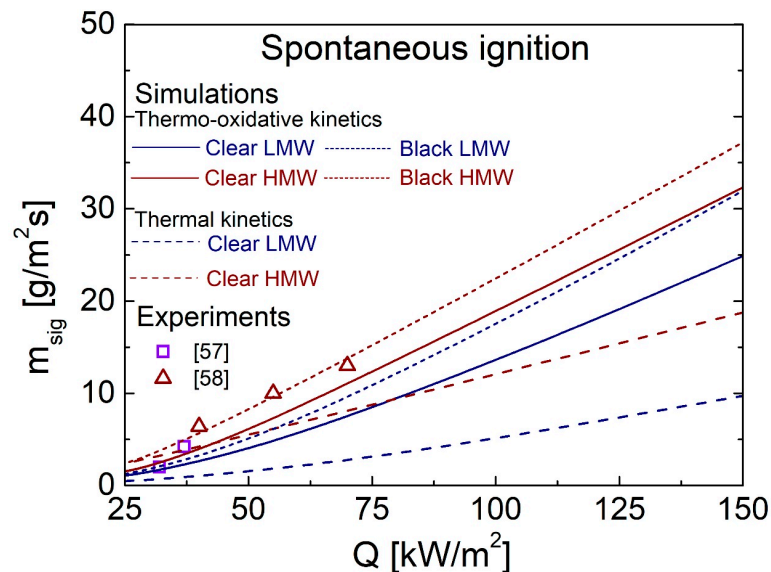


Figure 12. Surface mass flux at ignition, m_{sig} , vs. heat flux, Q , as predicted for clear and black LMW (solid and dotted blue lines) and HMW (solid and dotted brown lines) PMMA with thermo-oxidative decomposition kinetics and for clear LMW (dashed blue line) and HMW (dashed brown line) PMMA with purely thermal decomposition kinetics. Several experimental data (symbols) derived from the literature are also reported. (See Refs. [57,58]).

The acceptable agreement is also obtained between measured and predicted spontaneous T_{sig} for clear LMW PMMA. In this case, the agreement is better when thermal kinetics is used, but temperatures predicted with thermo-oxidative kinetics are lower by only 30–60 K. Much lower temperatures are predicted for the HMW PMMA in the range of 490–560 K, confirming that the measurements do not refer to samples with high molecular weight.

Only a few measurements are available for m_{sig} and for heat fluxes below 70 kW/m^2 . It seems that the agreement between measurements and predictions is better when the

decomposition kinetics for the HMW PMMA is considered. However, ignition surface temperatures and mass fluxes vary very rapidly once ignition conditions are attained, and thus, small delays in measurements may lead to overestimated values.

5. Conclusions

In this study, the effects of the molecular weight, decomposition kinetics (either purely thermal or thermo-oxidative), and optical properties of PMMA on the piloted and the spontaneous ignition characteristics are assessed using an unsteady one-dimensional condensed-gas mathematical model, previously developed and validated. The analysis is focused on two PMMA samples with a molecular weight of 10^6 g/mol (HMW PMMA) and 10^5 g/mol (LMW PMMA), characterized by a four-step and a single-step decomposition mechanism, respectively, in both nitrogen and air. The effects of the different optical properties are studied by considering clear and black PMMA.

The main ignition parameters predicted for the piloted ignition of black LMW and HMW PMMA with purely thermal and thermo-oxidative kinetics follow the same qualitative trends in the range of heat flux 25–150 kW/m². More specifically, t_{ig} , δ_{ig} , and w_{ig} decrease while T_{sig} , m_{sig} , and r_{ig} increase. The ignition position, x_{ig} , is generally very close to the spark position while T_{gmaxig} initially increases due to reduced activity of the combustion reaction in the preignition stage and then decreases, showing that the MMA combustion rate is sufficiently high to also activate ignition at lower temperatures and with smaller widths of the combustion zone.

The effects of the different polymer molecular weights on the prediction of the ignition times decrease when the heat flux increases, due to a progressively less important role of the decomposition kinetics with respect to the transport phenomena. In fact, the t_{ig} values predicted for the HMW PMMA are lower by factors of 2.8–1.6 with respect to the other case. The predicted surface temperature, T_{sig} , is lower by about 90–70 K, while the mass flux, m_{sig} , is higher by a nearly constant factor of about 1.3.

Smaller effects are observed for purely thermal decomposition kinetics, compared with thermo-oxidative kinetics, with ignition times longer by a factor of 1.4–1.3 for the LMW PMMA and shorter by a factor of 1.3–1.2 for the HMW PMMA. At high heat fluxes, due to the reduced thickness of the flame, larger variations are predicted for the LMW PMMA on m_{sig} (up to a factor of 3.4), T_{sig} (up to about 45 K), and r_{ig} (up to a factor of 3.2).

Due to the absence of a pilot, spontaneous ignition occurs where adequate thermal and chemical conditions are reached. In the heat flux range of 25–150 kW/m², the main ignition variables follow the same qualitative trend observed for the piloted ignition, except for T_{gmaxig} and x_{ig} . The ignition time, t_{ig} , predicted for the HMW PMMA with thermo-oxidative decomposition kinetics is shorter by a factor of 1.8–1.3 with respect to the other case. The corresponding surface temperature, T_{sig} , is lower by about 60–70 K, while the mass flux, m_{sig} , is higher by a factor of 1.9–1.2 and T_{gmaxig} is lower by 20–50 K.

The comparison of the main spontaneous ignition variables predicted using thermal decomposition kinetics with respect to thermo-oxidative kinetics for the LMW PMMA shows that the ignition time, t_{ig} , is longer by factors of about 1.4–1.2. The surface temperature T_{sig} is higher by about 30 K–60 K and the predicted mass loss flux, m_{sig} , is lower by factors 2.2–2.4. Smaller differences are predicted for the HMW PMMA.

Results predicted for clear PMMA are qualitatively similar to those predicted for black PMMA. The effects of the optical properties are independent of the molecular weight, and in the range of heat fluxes 25–150 kW/m², larger deviations are predicted at high heat fluxes. Longer t_{ig} , by factors of up to 1.3, and smaller m_{sig} and r_{ig} , up to factors of about 2.0, are predicted, while differences are negligible for other variables.

A good agreement is found between the predicted and the measured ignition times for both PMMA samples, although only a few data are available for the case of high molecular weight samples. Further measurements, also including the gas-phase temperature and the species mass fractions, would be useful for a more complete validation of the model. The exact specification of the experimental conditions and the specimen properties

is also a prerequisite for correct analysis. Moreover, the study of the ignition of other polymeric materials could also contribute to further understanding of this complex phenomenon. Finally, it is highly desirable that both new experiments and new models should be focused on the conditions of real fires by considering variable external heat fluxes and convective flow.

Supplementary Materials: The following supporting information can be downloaded at: <https://www.mdpi.com/article/10.3390/pr12010219/s1>, Table S1. Model equations for the solid and the gas phase with initial and boundary conditions; Table S2. Equations for the solid and gas properties; Table S3. Model equations and schematization of the spark.

Author Contributions: Conceptualization, A.G. and C.D.B.; data curation, A.G. and C.D.B.; formal analysis, A.G. and C.D.B.; investigation, A.G. and C.D.B.; methodology, A.G. and C.D.B.; project administration, A.G. and C.D.B.; resources, C.D.B.; software, A.G.; validation, A.G.; visualization, A.G. and C.D.B.; writing—original draft, A.G. and C.D.B.; writing—review and editing, A.G. and C.D.B. All authors have read and agreed to the published version of the manuscript.

Funding: This research received no external funding.

Data Availability Statement: Data are contained within the article or Supplementary Materials.

Conflicts of Interest: The authors declare no conflicts of interest.

References

1. Patel, N.; Sivanathan, K.; Mhaskar, P. Polymethyl Methacrylate Quality Modeling with Missing Data Using Subspace Based Model Identification. *Processes* **2021**, *9*, 1691. [[CrossRef](#)]
2. Jayarama Krishna, J.V.; Srivatsa Kumar, S.; Korobeinichev, O.P.; Vinu, R. Detailed kinetic analysis of slow and fast pyrolysis of poly(methylmethacrylate)-Flame retardant mixtures. *Thermochim. Acta* **2020**, *687*, 178545. [[CrossRef](#)]
3. Ding, Y.; Zhang, W.; Zhang, X.; Han, D.; Liu, W.; Ji, J. Pyrolysis and combustion behavior study of PMMA waste from micro-scale to bench-scale experiments. *Fuel* **2022**, *319*, 123717. [[CrossRef](#)]
4. Yang, C.; Shang, H.; Li, J.; Fan, X.; Sun, J.; Duan, A. A Review on the Microwave-Assisted Pyrolysis of Waste Plastics. *Processes* **2023**, *11*, 1487. [[CrossRef](#)]
5. Slavu, N.; Dinca, C. Clean Energy from Poplar and Plastic Mix Valorisation in a Gas Turbine with CO₂ Capture Process. *Processes* **2023**, *11*, 2922. [[CrossRef](#)]
6. Di Blasi, C. The state of the art of transport models for charring solid degradation. *Polym. Int.* **2000**, *49*, 1133–1146. [[CrossRef](#)]
7. Galgano, A.; Di Blasi, C. One-dimensional modeling approaches for the piloted ignition of poly(methyl methacrylate). *Fire Safety J.* **2022**, *129*, 103566. [[CrossRef](#)]
8. Galgano, A.; Di Blasi, C. Assessment of the predictive capabilities of a solid-gas model for poly (methyl methacrylate) ignition. *Fire Safety J.* **2024**, *142*, 104041. [[CrossRef](#)]
9. van Blijderveen, M.; Bramer, E.A.; Brem, G. Modelling piloted ignition of wood and plastics. *Waste Manag.* **2012**, *32*, 1659–1668. [[CrossRef](#)]
10. Stoliarov, S.I.; Crowley, S.; Lyon, R.E.; Linteris, G.P. Prediction of the burning rates of non-charring polymers. *Combust. Flame* **2009**, *156*, 1068–1083. [[CrossRef](#)]
11. Bal, N.; Rein, G. Numerical investigation of the ignition delay time of a translucent solid at high radiant heat fluxes. *Combust. Flame* **2011**, *158*, 1109–1116. [[CrossRef](#)]
12. Patel, A.; Hull, R.R.; Stec, A.A.; Lyon, R.E. Influence of physical properties on polymer flammability in the cone calorimeter. *Polym. Advan Technol.* **2011**, *22*, 1100–1107. [[CrossRef](#)]
13. Linteris, G.T. Numerical simulations of polymer pyrolysis rate: Effect of property variations. *Fire Mater.* **2011**, *35*, 463–480. [[CrossRef](#)]
14. Leventon, I.T.; Jing, L.; Stoliarov, S.I. A flame spread simulation based on a comprehensive solid pyrolysis model coupled with a detailed empirical flame structure representation. *Combust. Flame* **2015**, *162*, 3884–3895. [[CrossRef](#)]
15. Vermesi, I.; Roenner, N.; Pironi, P.; Hadden, R.M.; Rein, G. Pyrolysis and ignition of a polymer by transient irradiation. *Combust. Flame* **2016**, *163*, 31–41. [[CrossRef](#)]
16. Gong, J.; Chen, Y.; Jiang, J.; Yang, L.; Li, J. A numerical study of thermal degradation of polymers: Surface and in-depth absorption. *Appl. Therm. Eng.* **2016**, *106*, 1366–1379. [[CrossRef](#)]
17. Galgano, A.; Branca, C.; Di Blasi, C.; Vollaro, P.; Milella, E. Modeling the ignition of poly(methyl methacrylate)/carbon nanotube nanocomposites. *Polym. Degrad. Stabil.* **2017**, *144*, 344–353. [[CrossRef](#)]
18. Snegirev, A.; Kuznetsov, E.; Markus, E. Coupled analytical approach to predict piloted flaming ignition of non-charring polymers. *Fire Saf. J.* **2017**, *93*, 74–83. [[CrossRef](#)]

19. Gong, J.; Zhang, M.; Zhai, C.; Yang, L.; Wang, Y.Z.Z. Experimental, analytical and numerical investigation on auto-ignition of thermally intermediate PMMA imposed to linear time-increasing heat flux. *Appl. Therm. Eng.* **2020**, *172*, 115137. [[CrossRef](#)]
20. Kashiwagi, T. A radiative ignition model of a solid fuel. *Combust. Sci. Technol.* **1974**, *8*, 225–236. [[CrossRef](#)]
21. Di Blasi, C.; Crescitelli, S.; Russo, G.; Cinque, G. Numerical model of ignition processes of polymeric materials including gas phase absorption of radiation. *Combust. Flame* **1991**, *83*, 333–344. [[CrossRef](#)]
22. Brescianini, C.P.; Yeoh, G.H.; Chandrasekaran, V.; Yuen, R. A numerical model for pilot ignition of PMMA in a cone calorimeter. *Combust. Sci. Technol.* **1997**, *129*, 321–345. [[CrossRef](#)]
23. Tsai, T.H.; Li, M.J.; Shih, I.Y.; Jih, R.; Wong, S.C. Experimental and numerical study of autoignition and pilot ignition of PMMA plates in a cone calorimeter. *Combust. Flame* **2001**, *124*, 466–480. [[CrossRef](#)]
24. Nakamura, Y.; Kashiwagi, T. Effects of sample orientation on nonpiloted ignition of thin poly(methyl methacrylate) sheet by a laser. 1. Theoretical prediction. *Combust. Flame* **2005**, *141*, 149–169. [[CrossRef](#)]
25. Esfahani, J.A.; Kashani, A. One-dimensional numerical model for degradation and combustion of polymethyl methacrylate. *Heat Mass. Transfer* **2006**, *42*, 569–576. [[CrossRef](#)]
26. Wang, X.; Wang, X.; Cui, J.; Wang, X.; Zhang, J. Theoretical calculation on the piloted ignition of PMMA. *J. Macromol. Sci. B* **2007**, *46*, 475–485. [[CrossRef](#)]
27. Fereres, S.; Lautenberger, C.; Fernandez-Pello, A.C.; Urban, D.L.; Ruff, G.A. Understanding ambient pressure effects on piloted ignition through numerical modeling. *Combust. Flame* **2012**, *159*, 3544–3553. [[CrossRef](#)]
28. Peng, F.; Zhou, X.D.; Zhao, K.; Wu, Z.B.; Yang, L.Z. Experimental and numerical study on effect of sample orientation on auto-ignition and piloted ignition of poly(methyl methacrylate). *Materials* **2015**, *8*, 4004–4021. [[CrossRef](#)]
29. Wang, X.; Zhou, T.; Chen, Q.; Wang, J. Numerical study on the effect of oxygen concentration on the piloted ignition of PMMA in reduced pressure atmospheres. *Int. J. Numer. Method. Heat Fluid Flow* **2020**, *30*, 3903–3917. [[CrossRef](#)]
30. Korobeinichev, O.P.; Paletsky, A.A.; Gonchikzhapov, M.B.; Glaznev, R.K.; Gerasimov, I.E.; Naganovsky, Y.K.; Shundrina, I.K.; Snegirev, A.Y.; Vinu, R. Kinetics of thermal decomposition of PMMA at different heating rates and in a wide temperature range. *Thermochim. Acta* **2019**, *671*, 17–25. [[CrossRef](#)]
31. Chang, T.C.; Yu, P.Y.; Hong, Y.S.; Wu, T.R.; Chiu, Y.S. Effect of phenolic phosphite antioxidant on the thermo-oxidative degradation of PMMA. *Polym. Degrad. Stabil.* **2002**, *77*, 29–34. [[CrossRef](#)]
32. Di Blasi, C.; Galgano, A.; Branca, C. Modeling the thermal degradation of poly(methyl methacrylate)/carbon nanotube nanocomposites. *Polym. Degrad. Stabil.* **2013**, *98*, 266–275. [[CrossRef](#)]
33. Kang, B.S.; Kim, S.G.; Kim, J.S. Thermal degradation of poly(methyl methacrylate) polymers: Kinetics and recovery of monomers using a fluidized bed reactor. *J. Anal. Appl. Pyrol.* **2008**, *8*, 7–13. [[CrossRef](#)]
34. Ferriol, M.; Gentilhomme, A.; Cochez, M.; Oget, N.; Mieloszynski, J.L. Thermal degradation of poly(methyl methacrylate) (PMMA): Modelling of DTG and TG curves. *Polym. Degrad. Stabil.* **2003**, *79*, 271–281. [[CrossRef](#)]
35. Hirata, T.; Kashiwagi, T.; Brown, J.E. Thermal and oxidative degradation of poly(methylmethacrylate): Weight loss. *Macromolecules* **1985**, *18*, 1410–1418. [[CrossRef](#)]
36. Fina, A.; Camino, G. Ignition mechanisms in polymers and polymer nano-composites. *Polym. Adv. Technol.* **2011**, *22*, 1147–1155. [[CrossRef](#)]
37. Manring, L.E.; Sogah, D.Y.; Cohen, G.M. Thermal degradation of poly(methyl-methacrylate). 3. Polymer with head-to-head linkages. *Macromolecules* **1989**, *22*, 4652–4654. [[CrossRef](#)]
38. Amos, B.; Fernandez-Pello, A.C. Model of the ignition and flame development on a vaporizing combustible surface in a stagnation point flow: Ignition by vapor fuel radiation absorption. *Combust. Sci. Technol.* **1988**, *62*, 331–343. [[CrossRef](#)]
39. Wilke, C.R.; Lee, C.Y. Estimation of diffusion coefficients for gases and vapors. *Ind. Eng. Chem.* **1955**, *47*, 1253–1257. [[CrossRef](#)]
40. Perry, R.H.; Green, D.W.; Maloney, J.O. *Perry's Chemical Engineers' Handbook*, 6th ed.; McGraw-Hill: New York, NY, USA, 1984.
41. Stoliarov, S.I.; Walters, R.N. Determination of the heats of gasification of polymers using differential scanning calorimetry. *Polym. Degrad. Stabil.* **2008**, *93*, 422–427. [[CrossRef](#)]
42. Linteris, G.; Zammarano, M.; Wilthan, B.; Hanssen, L. Absorption and reflection of infrared radiation by polymers in fire-like environments. *Fire Mater.* **2012**, *36*, 537–553. [[CrossRef](#)]
43. Luche, J.; Rogaume, T.; Richard, F.; Guillaume, E. Characterization of thermal properties and analysis of combustion behaviour of PMMA in a cone calorimeter. *Fire Saf. J.* **2011**, *46*, 451–461. [[CrossRef](#)]
44. Lyon, R.E.; Quintiere, J.G. Criteria for piloted ignition of combustible solids. *Combust. Flame* **2007**, *151*, 551–559. [[CrossRef](#)]
45. Babrauskas, V.; Parker, W. Ignitability measurements with cone calorimeter. *Fire Mater.* **1987**, *11*, 31–43. [[CrossRef](#)]
46. Thompson, H.E.; Drysdale, D.D. Effect of sample orientation on the piloted ignition of PMMA. In Proceedings of the 5th International Conference Interflam '90, Canterbury, UK, 3–6 September 1990.
47. Rhodes, B.T. Burning Rate and Flame Heat Flux for PMMA in the Cone Calorimeter. Master's Thesis, Grant/Contract Reports (NISTGCR), National Institute of Standards and Technology, University of Maryland, Gaithersburg, MD, USA, 1994.
48. Hopkins, D., Jr.; Quintiere, J.G. Material fire properties and predictions for thermoplastics. *Fire Safety J.* **1996**, *26*, 241–268. [[CrossRef](#)]
49. Cordova, J.L.; Walther, D.C.; Torero, J.L.; Fernandez-Pello, A.C. Oxidizer flow effects on the flammability of solid combustibles. *Combust. Sci. Technol.* **2001**, *164*, 253–278. [[CrossRef](#)]

50. Dakka, S.M.; Jackson, G.S.; Torero, J.L. Mechanisms controlling the degradation of poly(methylmethacrylate) prior to piloted ignition. *Proc. Combust. Inst.* **2002**, *29*, 281–287. [[CrossRef](#)]
51. Beaulieu, P.A.; Dembsey, N.A. Flammability characteristics at applied heat flux levels up to 200 kW/m². *Fire Mater.* **2008**, *32*, 61–86. [[CrossRef](#)]
52. Kashiwagi, T. Experimental observation of radiative ignition mechanisms. *Combust. Flame* **1979**, *34*, 231–244. [[CrossRef](#)]
53. Long, R.T., Jr.; Torero, J.L.; Quintiere, J.G.; Fernandez-Pello, A.C. Scale and transport considerations on piloted ignition of PMMA. In *Fire Safety Science—Proceedings of the 6th International Symposium*; International Association for Fire Safety Science: London, UK, 1999.
54. Beaulieu, P.A. Flammability Characteristics at Heat Flux Levels Up to 200 KW/m² and the Effect of Oxygen on Flame Heat Flux. Ph.D. Thesis, Worcester Polytechnic Institute, MA, USA, 2005.
55. Shi, L.; Chew, M.Y.L. Fire behaviors of polymers under autoignition conditions in a cone calorimeter. *Fire Safety J.* **2013**, *61*, 243–253. [[CrossRef](#)]
56. Kashiwagi, T. Effects of sample orientation on radiative ignition. *Combust. Flame* **1982**, *44*, 223–245. [[CrossRef](#)]
57. Zhou, Y.; Lizhong, Y.; Jiakun, D.; Yafei, W.; Zhihua, D. Radiation attenuation characteristics of pyrolysis volatiles of solid fuels and their effect for radiation ignition model. *Combust. Flame* **2010**, *157*, 167–175. [[CrossRef](#)]
58. Huang, D.; Wang, C.; Shen, Y.; Lin, P.; Shi, L. Fire behaviors of vertical and horizontal polymethyl methacrylate slabs under autoignition conditions. *Process Saf. Prog.* **2020**, *39*, e12109. [[CrossRef](#)]

Disclaimer/Publisher’s Note: The statements, opinions and data contained in all publications are solely those of the individual author(s) and contributor(s) and not of MDPI and/or the editor(s). MDPI and/or the editor(s) disclaim responsibility for any injury to people or property resulting from any ideas, methods, instructions or products referred to in the content.